GLOBAL HEALTH SYNAPSE

ISSN:3059-7447

# Modeling and Simulation of the Dynamics of Fluid Flow and Heat Transfer for MRI-Guided Hyperthermia Treatment

**ANNORD MWAPINGA**

Mwenge Catholic University: Department of Natural Sciences and Information Technology
P.O. Box 1226 Moshi-Tanzania

**How to cite this article:** Modeling and Simulation of the Dynamics of Fluid Flow and Heat Transfer for MRI-Guided Hyperthermia Treatment.(2024). Global Health Synapse, 1(1), 40-56
https://www.globalhealthsynapse.com/index.php/journal/article/view/8. **https://doi.org/10.63456/ghs-1-1-8**

***Abstract***

The current study modeled and simulated the dynamics of fluid flow and heat transfer for MRI- guided hyperthermia treatment. The blood flow along the artery was assumed to follow a New- tonian character. In the mathematical formulation, the flow was considered unsteady, laminar, incompressible, unidirectional, axisymmetric, and fully developed. Additionally, the effects of induced magnetic fields and Hall effects were deemed negligible. The study found that blood velocity and temperature significantly varied with the enhancement of magnetic strength, Reynolds number, Grashof number, and heat source parameter. In contrast, blood velocity showed a gradual variation with increasing Prandtl number and Eckert number. This study holds significant value for medical applications, offering a means to simulate various scenar- ios and providing a controlled, reproducible environment to test different parameters, optimize heating strategies, and predict patient-specific treatment responses. The model developed can be used to predict treatment outcomes, identify potential complications, and suggest optimized treatment protocols tailored to the anatomical and physiological characteristics of individual patients.

**Key words**: Modeling, MRI, Thermal therapy fluid flow, Finite difference Scheme

## *Introduction*

Targeting tumor tissue with precision while minimizing damage to surrounding healthy tissue remains a significant challenge in the effectiveness of MRI-guided hyperthermia treatments. The complexity of blood flow, tissue properties, and heat transfer necessitates accurate simulation and modeling to optimize treatment delivery. Thermal therapy involves exposing the body to elevated temperatures beyond the normal range, a process commonly referred to as hyperthermia. Even a slight increase in temperature—just a few degrees above normal—can lead to substantial biological changes, including cell death. Research has shown that hyperthermia can be one of the most potent modifiers of radiation treatments. When used in cancer treatment, hyperthermia involves subjecting tissues to controlled high temperatures to damage or destroy cancer cells. This approach leverages the fact that cancer cells are generally more heat-sensitive than normal healthy cells. At temperatures between 40°C and 45°C, cancer cells experience significant stress, leading to the breakdown of proteins, membranes, and DNA, which ultimately results in cell death (apoptosis). Hyperthermia impacts cells and tissues in various ways, not only by directly altering the physical properties of cellular components but also by influencing cellular responses. Conventional cancer treatments such as radiotherapy and chemotherapy have limitations, and their effectiveness can be enhanced when combined with complementary therapies like hyperthermia, which can produce a synergistic effect when used alongside radiation and chemotherapy.

Magnetic Resonance Imaging (MRI) has become a crucial non-invasive imaging technique, with

applications across various fields such as biology, engineering, and material science. MRI is particularly valued for its ability to provide distinct contrast between soft tissues, often surpassing the quality of CT imaging. Research has shown that in the human body, oxygenated blood is diamagnetic, while deoxygenated blood is paramagnetic. As the oxygen level in the blood fluctuates, its magnetic susceptibility also changes, leading to alterations in the MRI signal. Blood is a complex fluid containing

a variety of ions—electrically charged particles that play a vital role in regulating processes such as fluid balance, nerve function, muscle contraction, and pH levels. In the presence of strong magnetic fields, the movement and behavior of these ions can be influenced by the magnetic forces, as they experience a Lorentz force due to their charge and motion within the field.

Numerous researchers have investigated fluid flow along the arterial wall. One study by [8] modeled the blood flow dynamics in a constricted artery during hyperthermia cancer treatment, though it did not account for the effects of the magnetic field. In contrast, [9] conducted a numerical study on tapered arteries, focusing on the transient simulation of non-Newtonian bio-magnetic fluid dynamics of blood flowing through a stenotic artery under the influence of a transverse magnetic field. Their findings indicated that the resistance to flow increases with both the height of the stenosis and the strength of the magnetic field. Similarly, [10] explored the flow of blood mixed with copper nanoparticles through an inclined, overlapping stenosed artery under a magnetic field, drawing similar conclusions regarding the impact of both stenosis and magnetic fields on flow resistance. [11] also examined the effect of a uniform magnetic field on pulsatile non-Newtonian blood flow in an elastic stenosed artery, although this study did not consider the stenosis itself. Other significant contributions to this area of research were made by [12], [13], [14], and [15], who also studied the role of magnetic fields in blood flow.Bottom of Form

To the best of my knowledge, the integration of fluid dynamics and heat transfer within the context of MRI-guided hyperthermia remains inadequately explored. Addressing this gap is crucial for establishing a more accurate and reliable framework for predicting thermal distribution, enhancing treatment planning, and ultimately improving therapeutic outcomes. This study seeks to overcome these limitations by formulating a comprehensive mathematical model that incorporates both fluid flow and heat transfer mechanisms.

***Model Formulation***

In this section we mathematically formulate the model. The following phases for model formulation were followed. See Fig. 1.

In formulating the model, the following assumptions were considered:

- The flow is unsteady, laminar, incompressible unidirectional, axisymmetric and full developed
- The fluid is Newtonian. In this regard, it is assumed that, the resistance to flow of the fluid is independent of the rate at which it is deformed.
- The flow is subjected to a uniform transverse magnetic field of strength $B_0$
- The induced magnetic fields and hall effects are negligible.
- Fluid flows in a cylindrical tube.

Following [17] we can write the geometry of stenosis as

$$H(z) = \begin{cases} d, & \text{for } \sigma \left(1 + \cos \dfrac{\pi z}{2z_0}\right) \\ 0, & \text{otherwise} \end{cases} \tag{2.1}$$

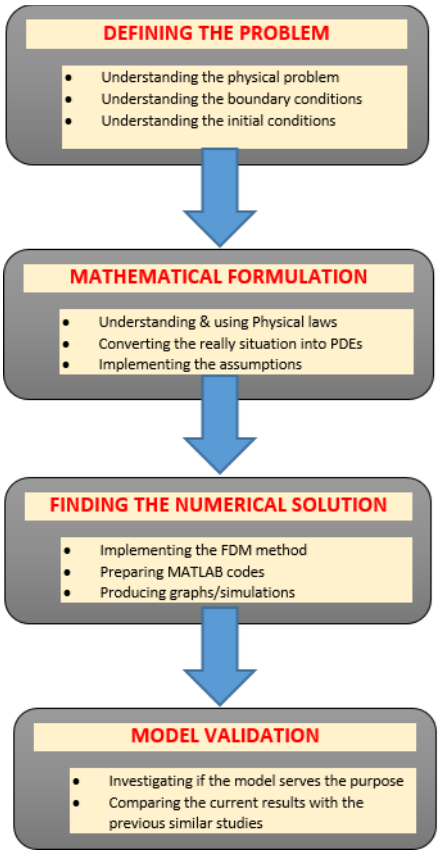


Figure 1: Phases of the Model Formulation

and the pressure gradient

$$-\frac{\partial P}{\partial z} = A_0 + A_1 \cos nt \tag{2.2}$$

where $H(z)$ is the radius of the constricted artery, $d$ is the radius of the normal artery, $4z_0$ is the length of stenosis, $2\sigma$ is the maximum protuberance of the stenotic form of the artery wall, $A_0$ is the steady state part of the pressure gradient, $A_1$ is the amplitude of the oscillatory part and $n = 2\pi f$ where $f$ is the heart pulse frequency.

Under mentioned considerations, the governing continuity, momentum and energy equations become:

$$\frac{\partial u}{\partial z} = 0 \tag{2.3}$$

$$\rho\frac{\partial u}{\partial t} = -\frac{\partial P}{\partial z} + \mu\left(\frac{1}{r}\frac{\partial u}{\partial r} + \frac{\partial^2 u}{\partial r^2}\right) - \sigma B_0^2 u + \beta_T(T - T_0) \tag{2.4}$$

$$\rho c_p\frac{\partial T}{\partial t} = k\left(\frac{1}{r}\frac{\partial T}{\partial r} + \frac{\partial^2 T}{\partial r^2}\right) + \mu\left(\frac{\partial u}{\partial r}\right)^2 + q_0(T - T_0) \tag{2.5}$$

Subject to the boundary and initial conditions

$$\frac{\partial u}{\partial r} = \frac{\partial T}{\partial r} = 0 \quad \text{at} \quad r = 0 \tag{2.6}$$

$$u(r, t) = 0, \quad T(r, t) = T_w \quad \text{at} \quad r = H(z) \tag{2.7}$$

$$u(r, 0) = f(r), \quad T(r, 0) = T_0 \tag{2.8}$$


Figure 2: Thermal-therapy treatment [16]

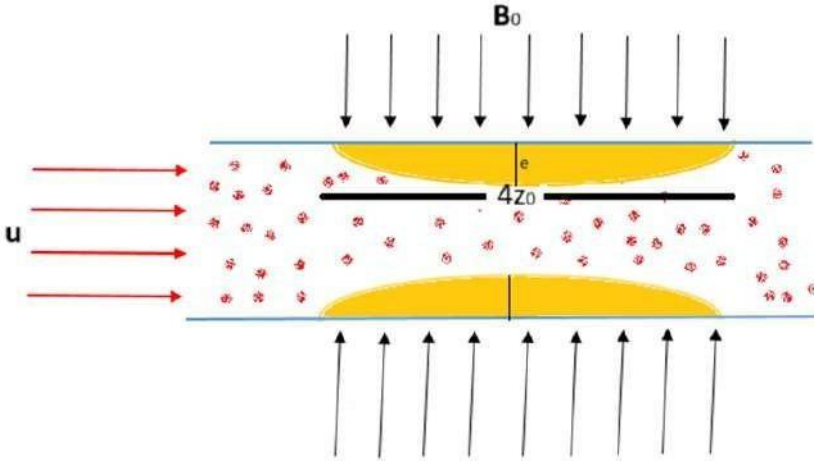


Figure 3: Geometry of the problem

For convenience, the following non-dimensional variables were introduced:

$$\theta = \frac{T - T_0}{T_w - T_0}, z^* = \frac{z}{z_0}, e^* = \frac{\sigma}{r}, u^* = \frac{u}{U}, \tau = \frac{tU}{d}, r^* = \frac{r}{d}$$
$$m = \frac{\rho d^2 n}{\mu}, \quad H^* = \frac{H(z)}{d}, \quad A_0 = A_0 \frac{\rho d^3}{\mu^2}, A_1 = A_1 \frac{\rho d^3}{\mu^2} \tag{2.9}$$

using eq. 2.9 in eqs. 2.3 – 2.8 we get the resulting equations in simplified form (dropping asterisks) as:

$$\frac{\partial u}{\partial z} = 0 \tag{2.10}$$

$$\frac{\partial u}{\partial \tau} = A_0 + A_1 \cos m\tau + \frac{1}{\mathrm{Re}} \frac{\partial^2 u}{\partial r^2} + \frac{1}{r_2} \frac{\partial u}{\partial r} - \frac{M^2}{\mathrm{Re}} u + \mathrm{Gr}\theta \tag{2.11}$$

$$\frac{\partial \theta}{\partial \tau} = \frac{1}{\mathrm{Pr}} \frac{\partial^2 \theta}{\partial r^2} + \frac{1}{r} \frac{\partial \theta}{\partial r} + \frac{\mathrm{Ec}}{\mathrm{Re}^2} \frac{\partial u}{\partial r} + Q\theta \tag{2.12}$$

where Re = $\frac{\rho a U}{\mu}$, Ec = $\frac{U^2}{c_p(T_w - T_0)}$, Pr = $\frac{c_p \mu}{k}$, $Q = \frac{q_0 d}{\rho c_p U}$ and Gr = $\frac{g\beta_T(T - T_0)\upsilon}{U^3}$ are respectively Reynolds number, Eckert number, Prandtl number, Heat source parameter, $M = B_0 U \sqrt{\frac{\sigma}{\mu}}$ Hartman number and Grashof number.

The dimensionless form of the stenosis geometry is given as

$$H(z) = \begin{cases} 1 - e \left[1 + \cos\left(\frac{\pi z}{2}\right)\right] & \text{if } -2 \le z \le 2 \\ 1 & \text{Otherwise} \end{cases} \tag{2.13}$$

Besides, the dimensionless form of the boundary and initial conditions become;

$$u(r, 0) = u_0, \quad T(r, 0) = T_0, \tag{2.14}$$

$$u(r, \tau) = T(r, \tau) = T_w \quad \text{on} \quad r = H(z) \tag{2.15}$$

$$\frac{\partial u(r, \tau)}{\partial r} = \frac{\partial T(r, \tau)}{\partial r} = 0 \quad \text{on} \quad r = 0 \tag{2.16}$$

***Solution of the Model Equations***

***Radial Coordinate Transformation***

In this section, we first introduce the radial coordinate transformation. The variable $\xi$ such that $\xi = \frac{r}{R(z)}$. This has an effect of immobilizing the arterial wall in the transformed coordinate $\xi$. Incorporating this transformation we get the following governing flow equations.

$$\frac{\partial u}{\partial \tau} = A_0 + A_1 \cos m\tau + \frac{1}{\mathrm{Re} H^2}\left(\frac{\partial^2 u}{\partial \xi^2} + \frac{1}{\xi}\frac{\partial u}{\partial \xi}\right) - \frac{M^2}{\mathrm{Re}} u + \mathrm{Gr}\theta \tag{3.1}$$

$$\frac{\partial \theta}{\partial \tau} = \frac{1}{\mathrm{Pr} H^2}\left(\frac{\partial^2 \theta}{\partial \xi^2} + \frac{1}{\xi}\frac{\partial \theta}{\partial \xi}\right) + \frac{\mathrm{Ec}}{\mathrm{Re}^2}\left(\frac{\partial u}{\partial \xi}\right)^2 + Q\theta \tag{3.2}$$

The boundary and initial conditions for the above equations become:

$$u(\xi, 0) = u_0, \quad \theta(\xi, 0) = \theta_0 \tag{3.3}$$

$$w(\xi, \tau) = 0 \quad \theta(\xi, \tau) = \theta_w, \quad \text{on} \quad \xi = 1 \tag{3.4}$$

$$\frac{\partial u(\xi, \tau)}{\partial \xi} = \frac{\partial \theta(\xi, \tau)}{\partial \xi} = 0 \quad \text{on} \quad \xi = 0 \tag{3.5}$$

Now using the axial velocity and the temperature of the streaming fluid we determine the the skin friction $C_f$ and the Nusselt number $Nu$ as follows:

$$C_f = \frac{1}{H}\frac{\partial u}{\partial \xi}\Big|_{\xi=1} \tag{3.6}$$

$$Nu = -\frac{1}{H}\frac{\partial \theta}{\partial \xi}\Big|_{\xi=1} \tag{3.7}$$

***Explicit Finite Difference Method***

The eqs. 3.1 − 3.7 are implemented using the well-known explicit finite difference method. Using this method we directly compute the solution at the next time step using known values

from the current time step, without the need to solve a system of equations. The explicit finite difference method is conditionally stable, meaning that the time step $\Delta\tau$ must be small enough to ensure stability. This condition is often related to the CFL condition (Courant-Friedrichs-Lewy condition), which constrains the relationship between the time step $\Delta\tau$ and the spatial step $\Delta\xi$ to prevent numerical instability. In this regard therefore, it was ensured that the condition $0 < \frac{\Delta\tau}{(\Delta\xi)^2} \leq 0.5$ is well taken into consideration. Besides, the Central difference formula is used to express the spatial derivatives and the forward difference formula is applied to the time derivatives. See equations below:

$$\frac{\partial u}{\partial \xi} = \frac{u_{i+1,j} - u_{i-1,j}}{2\Delta\xi}, \qquad \frac{\partial^2 u}{\partial \xi^2} = \frac{u_{i+1,j} + 2u_{i,j} - w_{i-1,j}}{(\Delta\xi)^2} \tag{3.8}$$

Similarly;

$$\frac{\partial \theta}{\partial \xi} = \frac{\theta_{i+1,j} - \theta_{i-1,j}}{2\Delta\xi}, \qquad \frac{\partial^2 \theta}{\partial \xi^2} = \frac{\theta_{i+1,j} + 2\theta_{i,j} - \theta_{i-1,j}}{(\Delta\xi)^2} \tag{3.9}$$

For time derivative we have:

$$\frac{\partial u}{\partial \tau} = \frac{u_{i,j+1} - u_{i,j}}{k}, \qquad \frac{\partial \theta}{\partial \tau} = \frac{\theta_{i,j+1} - \theta_{i,j}}{k} \tag{3.10}$$

We also define $\xi(i) = (i-i)\Delta\xi$ and $\tau_j = (j-1)\Delta\tau = (j-1)k$. Incorporating equations $3.8 - 3.10$ into eqs $3.1 - 3.7$ we have:

$$u_{i+1,j} = u_{i,j} + k(A_0 + A_1\cos(m\tau_j)) + \frac{k}{\mathrm{Re}H_i^2}\left(\frac{u_{i+1,j} + 2u_{i,j} - u_{i-1,j}}{(\Delta\xi)^2}\right) + \frac{k}{\mathrm{Re}H_i^2\eta_i}\left(\frac{u_{i+1,j} - u_{i-1,j}}{2\Delta\xi}\right) - \frac{M^2}{\mathrm{Re}}u_{i,j} + \mathrm{Gr}\theta_{i,j} \tag{3.11}$$

$$\theta_{i+1,j} = \theta_{i,j} + \frac{k}{\mathrm{Pr}H_i^2}\left(\frac{\theta_{i+1,j} + 2\theta_{i,j} - \theta_{i-1,j}}{(\Delta\xi)^2}\right) + \frac{k}{\mathrm{Pr}H_i^2\xi_i}\left(\frac{\theta_{i+1,j} - \theta_{i-1,j}}{2\Delta\xi}\right) + \frac{k\mathrm{Ec}}{(\mathrm{Re})^2H^2}\left(\frac{u_{i+1,j} - u_{i-1,j}}{2\Delta\xi}\right)^2 + Q\theta_{i,j} \tag{3.12}$$

Skin friction:

$$(C_f)_i = \frac{1}{H_i}\left(\frac{u_{i+1,j} - u_{i-1,j}}{2\Delta\xi}\right)\Bigg|_{\xi=1} \tag{3.13}$$

Nusselt number:

$$(Nu)_i = \frac{1}{H_i}\left(\frac{\theta_{i+1,j} - \theta_{i-1,j}}{2\Delta\xi}\right)\Bigg|_{\xi=1} \tag{3.14}$$

$\xi^{-1}$

***Graphical Results and Discussion***

In this section we discuss in a detail the effects of different parameters. Both velocity and temperature profiles are plotted and discussed. Besides, Reynolds, Hartman, Grashof, Prandtl and Eckert numbers were varied to see their effect on the profiles. skin friction and Nusselt

number are also simulated and discussed.

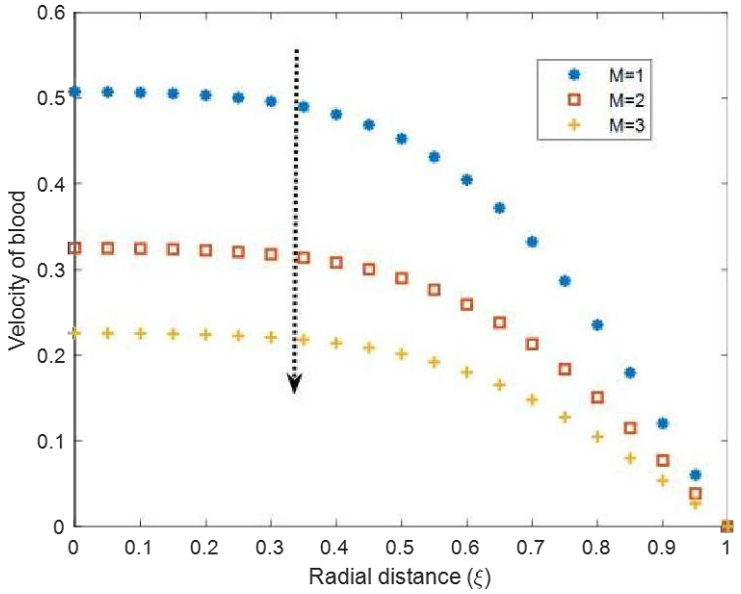


Figure 4: Effect of magnetic field on velocity profile

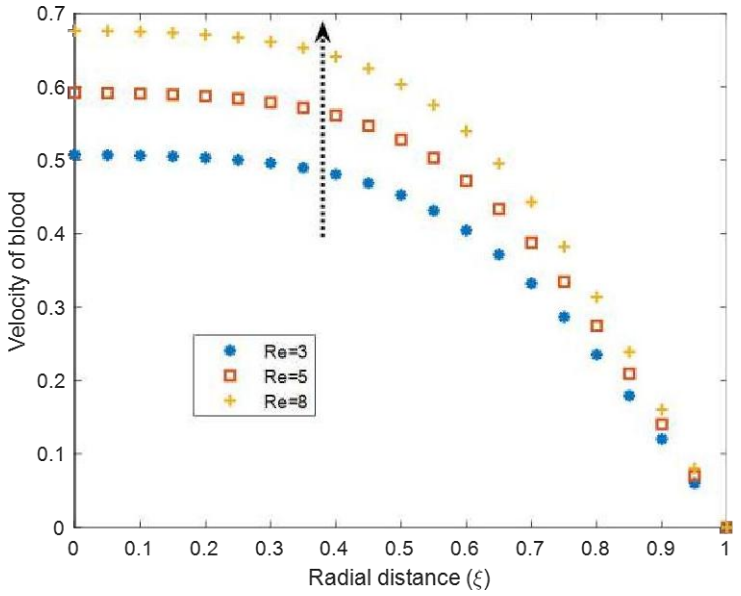


Figure 5

The effect of magnetic field on fluid's velocity is shown on Fig. 4. It is revealed that the blood's velocity decreases as the Hartman number increases. Physically, magnetic field exerts the Lorentz force which has the tendency to resist motion. This results to the decline in velocity. In this regard therefore, magnetic fields can be used practically in situations where the velocity of the blood need to be minimized. This include for example during post surgical recovery especially after vascular surgery. Reducing blood's velocity reduces the risk of complications such as bleeding. Fig. 5 shows the effect of increasing the Reynolds number on velocity. The reynolds number is a non-dimensional number which represents the ration of inertial force to viscous force. Increasing the Reynolds number implies the inertial force increases that viscous force. as the inertial force become more dominant than the viscous force, the blood's velocity

increases.

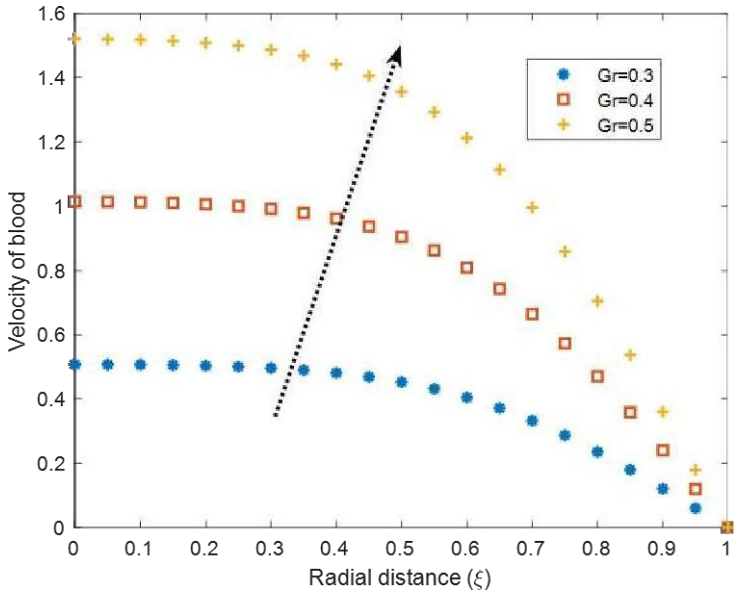


Figure 6: Effect of Grashof number on velocity profile

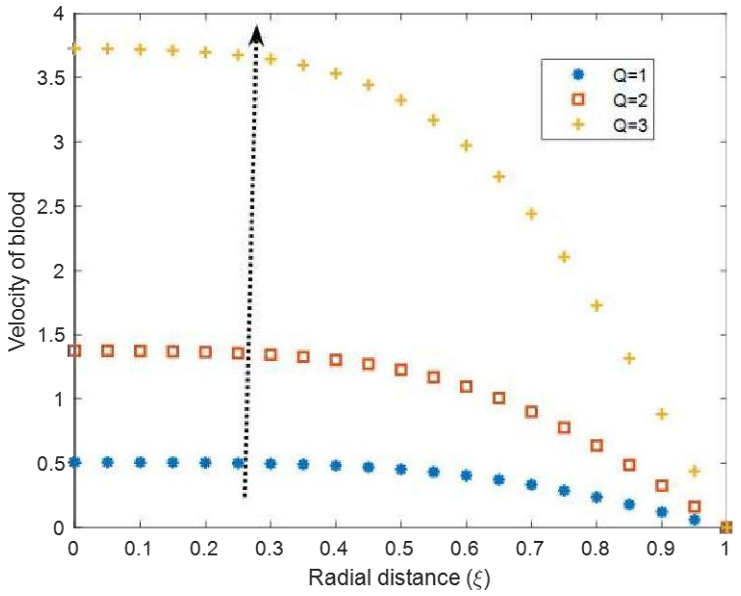


Figure 7: Effect of heat source parameter on velocity profile

Increase in Grashof number increases the velocity profile. This is shown on Fig. 6. Grashof number is a dimensionless number that quantifies the relative importance of buoyancy forces to viscous forces in a fluid flow, particularly in natural convection. When Grashof number increases, it promotes faster fluid motion as warmer, less dense blood rises or moves upward due to the buoyant force. The effect of heat source parameter Q is illustrated on Fig. 7. Increase in heat source parameter raises the temperature which in-turn, the raised temperature causes vasodilation (widening of blood vessels), which increases blood flow velocity. Vasodilation lowers the resistance to blood flow in the vessels, allowing blood to flow more easily. Prandtl number and Eckert number both have shown to enhance the velocity of blood. The Prandtl number is defined as the ratio of kinematic viscosity to thermal diffusivity. The effect of increasing

it, is shown on Fig. 8.The effect of Eckert number is shown on Fig. 9.

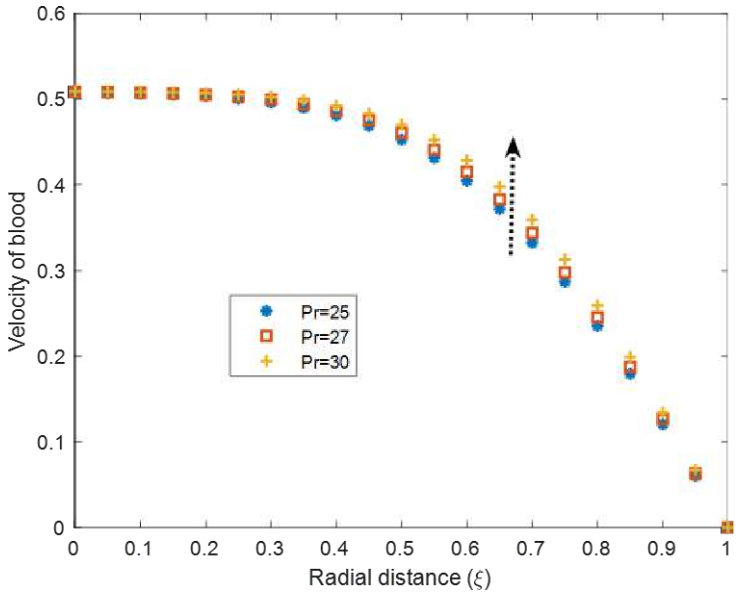


Figure 8: Effect of Prandtl number on velocity profile

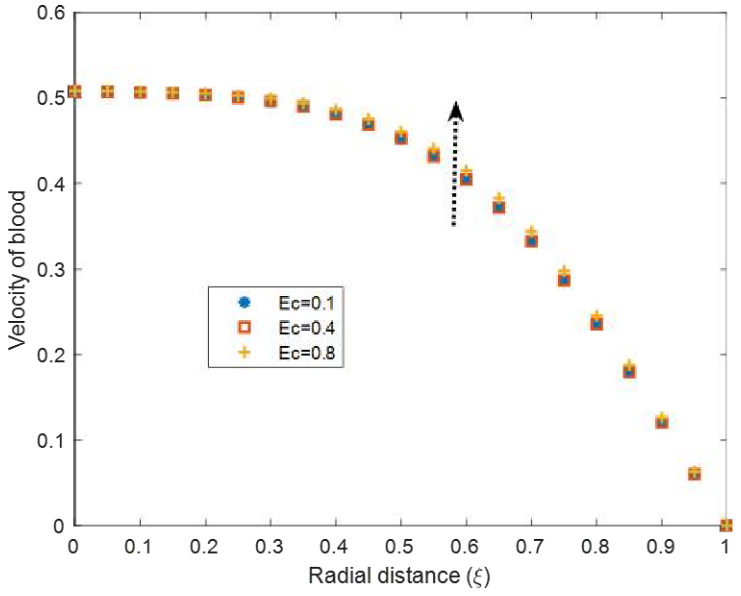


Figure 9: Effect of Eckert number on velocity profile

The Prandtl number is a measure of how a fluid behaves when it flows and how it transfers heat. It compares the thickness of the fluid's sticky layer, (this is always is related to viscosity) to the thickness of the layer where heat is transferred. Fig. 8 shows the effect of Prandtl number on velocity profile. It is observed that, the velocity is enhanced as the Prandtl number increases. Similar results was illustrated by [18]. The same is observed when Eckert number increases. The Eckert number is a dimensionless number that characterizes the relative importance of the kinetic energy of the fluid flow to its thermal energy. When Eckert number is increased, the flow is dominated by kinetic energy which increases the fluids velocity, that is an increase in the Eckert number leads to an increase in velocity because the flow becomes more dominated by kinetic energy and less by thermal energy. As the system becomes less efficient at transferring

heat (due to the imbalance between kinetic and thermal energy), the flow velocity tends to increase.

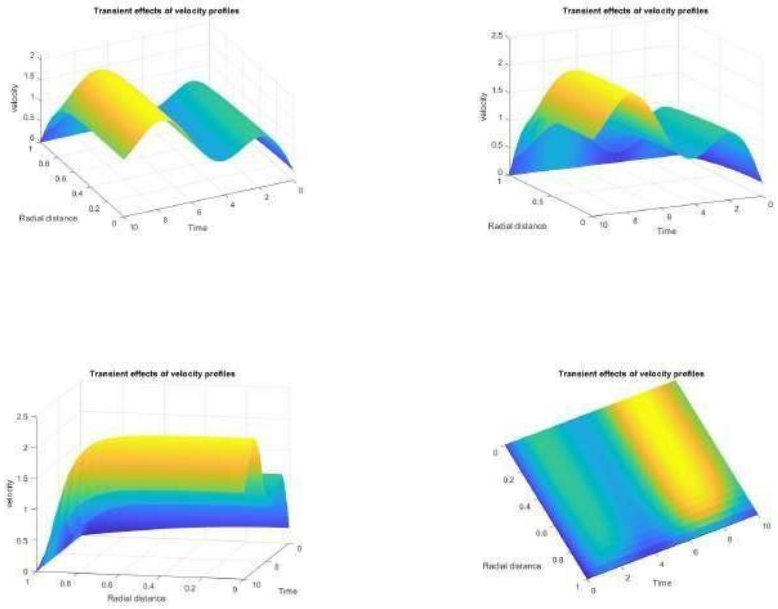


Figure 10: The transient effects of velocity profile

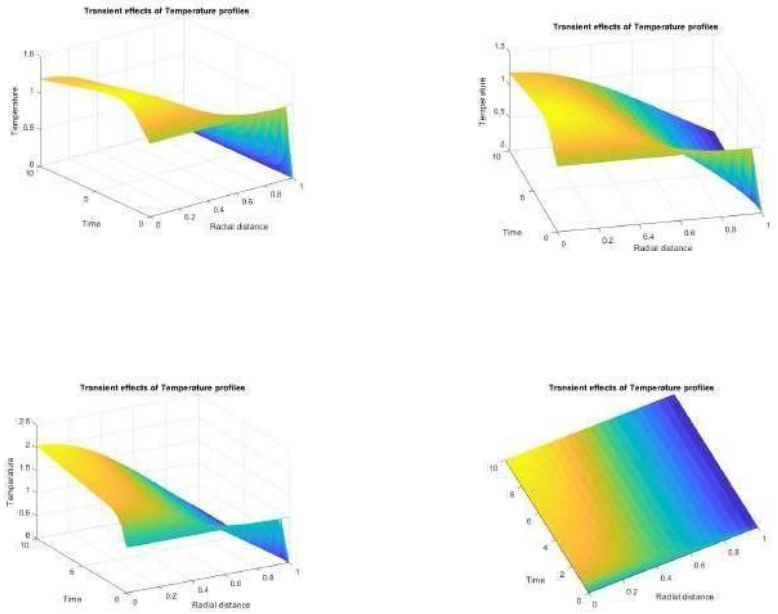


Figure 11: The transient effects of temperature profile

The transient effects of both velocity and temperature profiles are shown on Figs. 10 and 11. The graph show that the velocity decreases from the center of the artery radial distance $\xi = 0$ towards the arterial wall $\xi = 1$ where the velocity is zero. This is due to the fact that at the arterial wall, we have a no slip condition. Besides, it is shown that the velocity increases as time increases. This is due to the presence of heat source which enhances the flow velocity. On the other hand we see that temperature increases with time (see Fig. 11). The increase in temperature is due to the presence of the external heat source which directly enhances fluid's temperature. This temperature is responsible for killing the cancer cells.

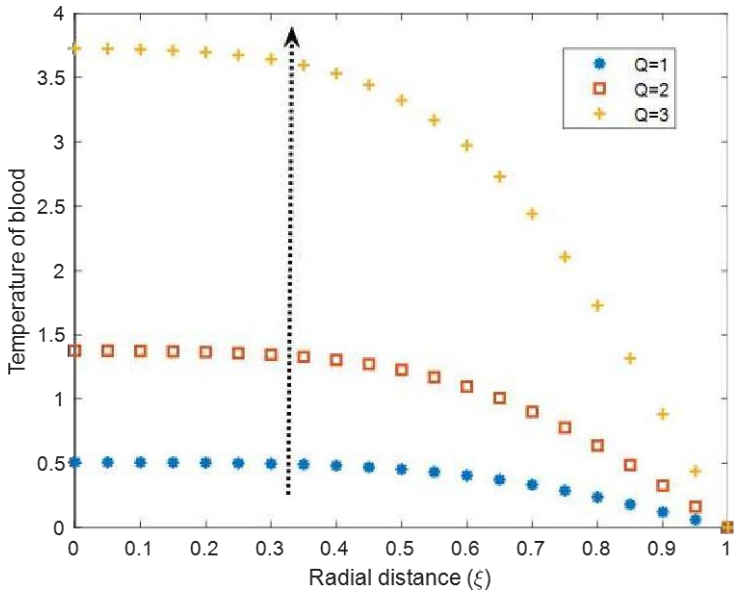


Figure 12

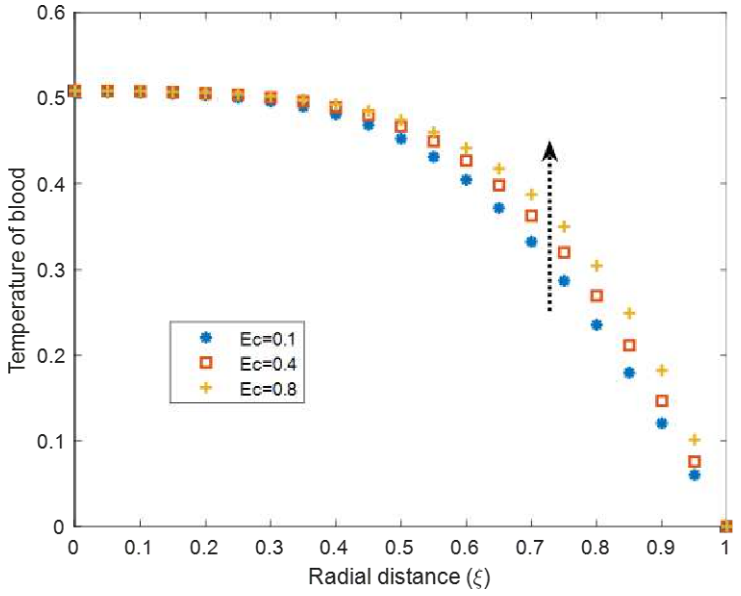


Figure 13

Figs. 12 and 13 portray the variation of temperature due to the changes in heat source and Eckert number respectively. In Fig. 12 we see that, as heat source parameter enhances, the temperature profile increases. As the intensity or temperature of the external heat source increases, more thermal energy is transferred into the blood, which results in an increase in the blood temperature. Besides, Fig. 13 we observe that similar situation when Eckert number increases. Increasing the Eckert number leads to the fluid's kinetic energy becoming more significant compared to its thermal energy. Such relationship suggests that as the velocity of the fluid increases, there is more dissipation of energy into heat, which can raise the local temperature.

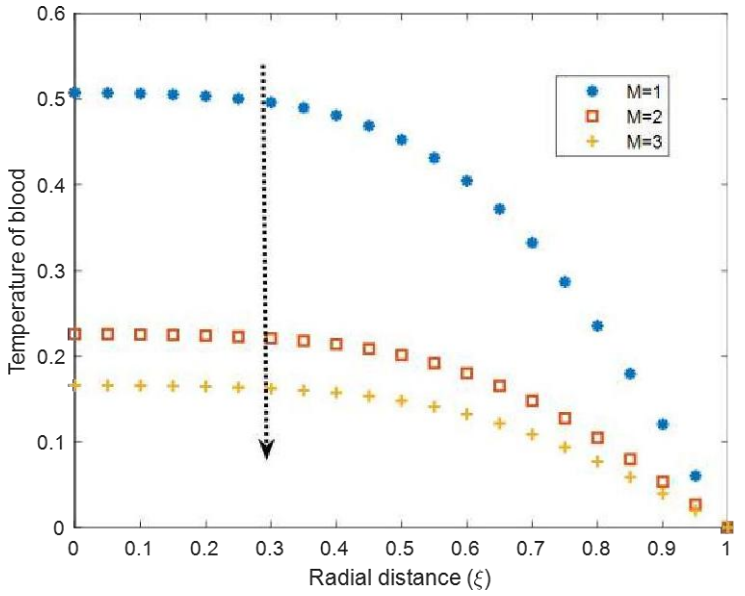


Figure 14

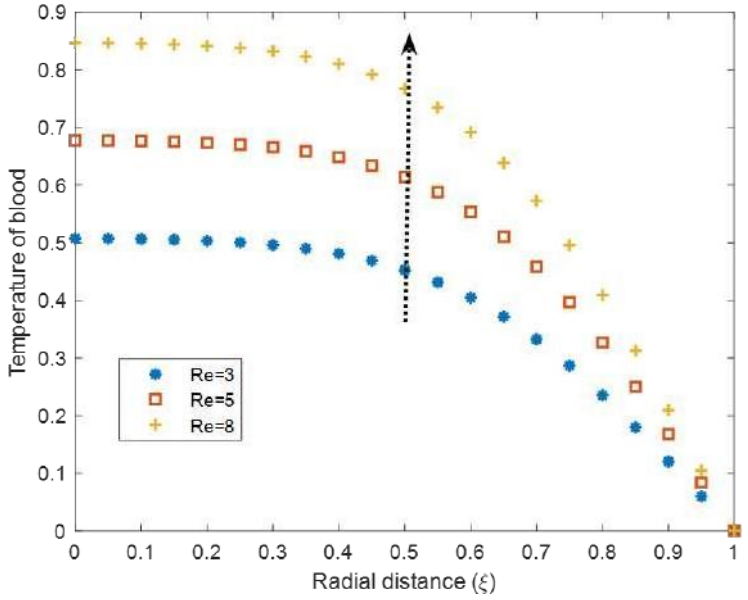


Figure 15

The effect of Magnetic parameter (Hartmann number) is shown in Fig. 14. The temperature is observed to diminish as magnetic strength increases. This is due to the fact that when the Hartmann number increases, the effects of the magnetic field become more significant compared to the viscous forces. In the presence of a strong magnetic field, the flow becomes more laminar, and the convective heat transfer is reduced because the magnetic field suppresses the fluid's movement. With an increase in Reynolds number, the velocity of the blood tends to increase as well. This increase in velocity means there is more kinetic energy in the system. This kinetic energy can be dissipated into heat via viscous dissipation. As the velocity of blood increases, more of this kinetic energy gets converted into heat, causing the temperature to rise. this is revealed in Fig. 15.

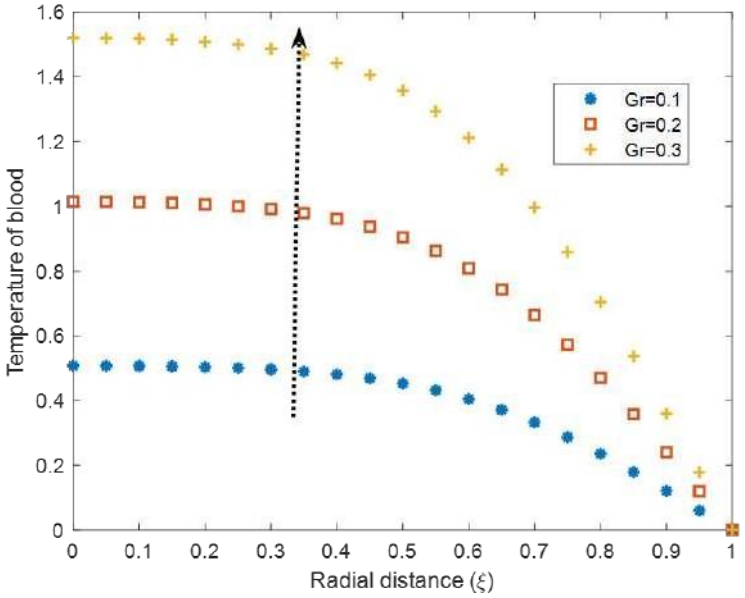


Figure 16

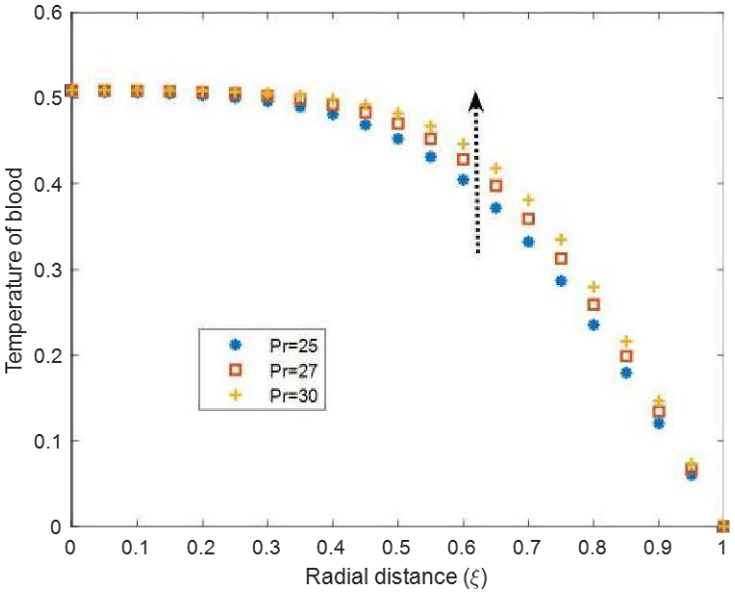


Figure 17

The effect of Grashof number on temperature is shown in Fig. [**?** ]. it is shown that as the Grashof number increases, the boundary layer (the thin region near the surface where temperature gradients are steep) becomes thicker, but the overall heat transfer improves due to stronger convective currents. The increased convection enhances the transport of heat, allowing the fluid to redistribute thermal energy more effectively. Fig. 17 shows the variation of temperature due to changes in Prandtl number. The temperature is observed to be enhanced as a result of increasing Prandtl number. Increasing the Prandtl number typically means that the fluid has a lower thermal diffusivity compared to its momentum diffusivity. This leads to thicker thermal boundary layers and a slower rate of heat transfer to or from the blood. As a result, the temperature may rises.

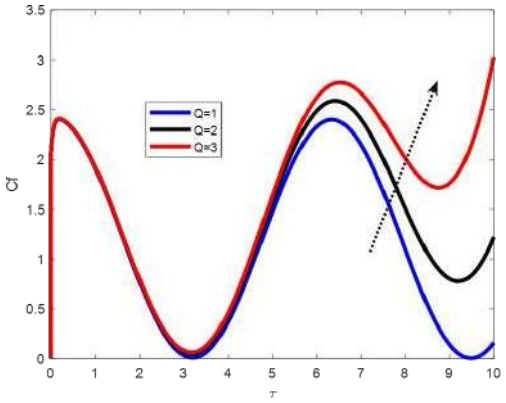


Figure 18: Effect of Q on *Cf*

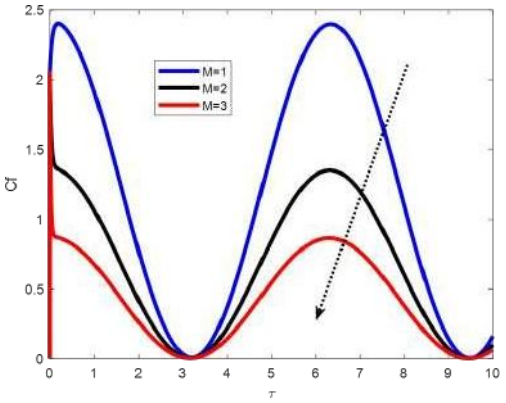


Figure 19: Effect of M on *Cf*

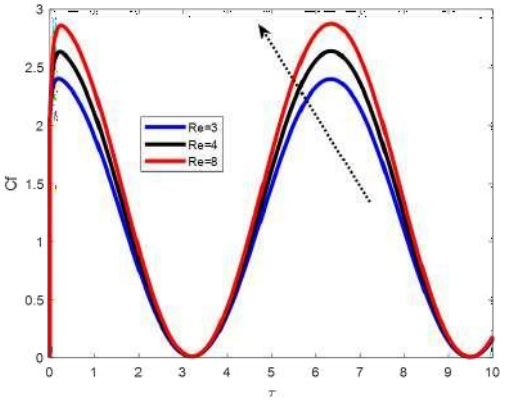


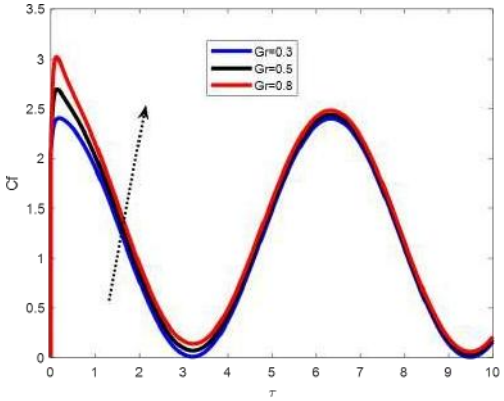


Figure 20: Effect of Re on *Cf* Figure 21: Effect of Gr on *Cf*

Skin friction refers to the shear stress exerted by a fluid on the surface it flows over, typically due to the viscosity of the fluid. This concept is crucial in understanding how fluids interact with surfaces. In blood flow, it plays an important role in determining the forces acting on the walls of blood vessels. Figs. 18− 21 show the dynamics of friction friction as a result of varying heat source parameter Q, Magnetic parameter M, Reynolds number Re, and the Grashof number Gr. It is shown that heat source parameter enhances the skin friction. As heat increases, sweat evaporation rates increases, leading to dry skin, which eventually increases friction. If the heat source is intense or prolonged, sweat evaporates too quickly or may not be produced at a sufficient rate, leading to dry skin, which increases skin friction, (see Fig. 18). Besides, Fig. 19 show different pattern when the Hartman number M increases. The skin friction is observed to decline with increasing in magnetic parameter M (The Hartman number). Magnetic fields can cause a reduction in fluid velocity near the skin surface due to the magneto-hydrodynamic effect (MHD). This lowers the skin shear stress, which directly correlates to a reduction in skin friction. Generally, the Hartman number is associated with the dominance of magnetic forces over viscous forces. As the Hartman number increases, it indicates that the magnetic forces are becoming more dominant relative to the viscous forces in the blood. The Skin friction is also observed to increase with increase in Reynolds number and Grashof number. see Figs. 20 and 21.

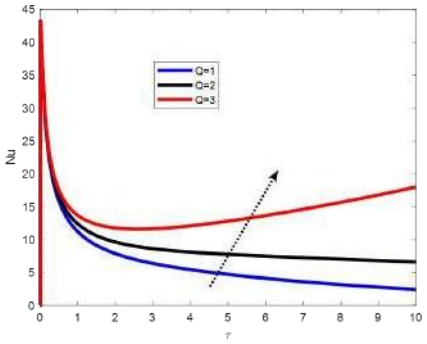


Figure 22: Effect of Q on $Nu$

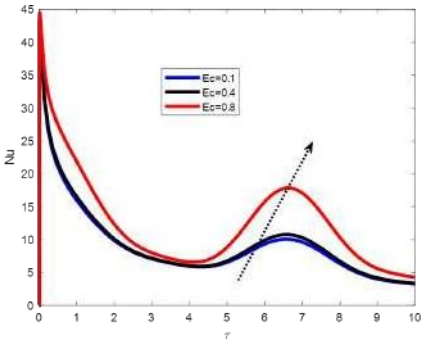


Figure 23: Effect of Ec on $Nu$

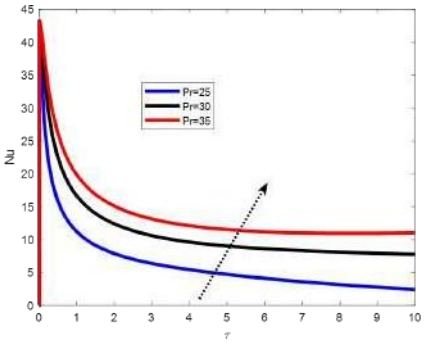


Figure 24: Effect of Pr on $Nu$

The Nusselt number (Nu) is a measure of how effectively heat is transferred by convection compared to heat transfer by conduction in a fluid. Figs (22 - 24) display the effect of varying heat source parameter, Eckert number and Prandtl number on Nusselt number. It is shown that, the Prandtl number increases with increase in heat source, Eckert number and Prandtl number. Fig. 22 we see that when the heat source intensifies, the convective heat transfer coefficient increases, which causes an increase in the Nusselt number. That is, if heat sources, it basically increases the thermal boundary layer thickness near the heat source. This generally increases the Nusselt number, since more heat is transferred from the surface into the blood. Fig. 23 reveals that, if Ec increases, the flow is becoming more energy-rich, so the convective heat transfer improves, and the Nusselt number increases. Besides,for higher Prandtl numbers, the Nusselt number tends to increase, as the thicker thermal boundary layer is less effective at transferring heat, leading to an increased convective heat transfer rate (See Fig. 24).

***Conclusion***

This study focused on the modeling and simulation of fluid flow dynamics and heat transfer in the context of MRI-guided hyperthermia treatment. The findings from the simulations provided valuable insights into the interplay between various parameters affecting both the velocity and temperature profiles within the system.

As anticipated, the velocity profile of blood was found to decrease with an increase in magnetic field strength. Conversely, an increase in the Reynolds number, Grashof number, heat source parameter, Prandtl number, and Eckert number led to an enhancement in blood velocity. Similarly, the temperature profile was observed to increase with higher values of the heat source parameter, Eckert number, Reynolds number, Grashof number, and Prandtl number. However, magnetic field strength exhibited an opposing effect, with higher magnetic strengths resulting in a reduction of the temperature profile.

In terms of skin friction and Nusselt number, similar trends were observed: both skin friction and Nusselt number increased with higher values of the heat source parameter, Eckert number, Reynolds number, Grashof number, and Prandtl number, while they decreased as magnetic strength increased. These results offer significant implications for optimizing hyperthermia treatment parameters in MRI-guided procedures, particularly in understanding the effects of magnetic field strength and thermal parameters on fluid dynamics and heat transfer. the Finite difference method was used to tackle the model equations, which were later simulated using MATLAB software.

***Conflicts of interest:***

The author declares that there are no known competing financial interests or personal relationships that could have influenced the work presented in this paper.

***References***

[1] S. Field and N. Bleehen, “Hyperthermia in the treatment of cancer,” Cancer treatment reviews, vol. 6, no. 2, pp. 63–94, 1979.

[2] H. Kampinga and E. Dikomey, “Hyperthermic radiosensitization: mode of action and clinical relevance,” International journal of radiation biology, vol. 77, no. 4, pp. 399–408, 2001.

[3] W. C. Numan, L. W. Hofstetter, G. Kotek, J. F. Bakker, E. W. Fiveland, G. C. Houston, G. Kudielka, D. T. Yeo, and M. M. Paulides, “Exploration of mr-guided head and neck hyperthermia by phantom testing of a modified prototype applicator for use with proton resonance frequency shift thermometry,” International Journal of Hyperthermia, vol. 30, no. 3, pp. 184–191, 2014.

[4] J. Crezee, N. A. Franken, and A. L. Oei, “Hyperthermia-based anti-cancer treatments,” 2021.

[5] K. Mortezaee, A. Narmani, M. Salehi, H. Bagheri, B. Farhood, H. Haghi-Aminjan, and M. Najafi, “Synergic effects of nanoparticles-mediated hyperthermia in radiotherapy/chemotherapy of cancer,” Life sciences, vol. 269, p. 119020, 2021.

[6] V. Kuperman, Magnetic resonance imaging: physical principles and applications. Elsevier, 2000.

[7] M. A. Syed, S. V. Raman, and O. P. Simonetti, Basic principles of cardiovascular MRI:

physics and imaging techniques. Springer, 2015.

[8] A. Mwapinga, “Mathematical modeling of the physics of blood flow along a constricted artery during treatment of cancer using hyperthermia,” Computational Mathematics and its Applications, pp. 010–017, 2024.

[9] M. Y. Abdollahzadeh Jamalabadi, M. Daqiqshirazi, H. Nasiri, M. R. Safaei, and T. K. Nguyen, “Modeling and analysis of biomagnetic blood carreau fluid flow through a steno- sis artery with magnetic heat transfer: A transient study,” PLoS One, vol. 13, no. 2,
p. e0192138, 2018.

[10] C. Umadevi, M. Dhange, B. Haritha, and T. Sudha, “Flow of blood mixed with copper nanoparticles in an inclined overlapping stenosed artery with magnetic field,” Case Studies in Thermal Engineering, vol. 25, p. 100947, 2021.

[11] M. R. Sadeghi, M. Jahangiri, and M. Saghafian, “The impact of uniform magnetic field on the pulsatile non-newtonian blood flow in an elastic stenosed artery,” Journal of the Brazilian Society of Mechanical Sciences and Engineering, vol. 42, pp. 1–15, 2020.

[12] N. M. Zain, Z. Ismail, and P. Johnston, “Numerical analysis of blood flow behaviour in a constricted porous bifurcated artery under the influence of magnetic field,” CFD Letters, vol. 15, no. 1, pp. 39–58, 2023.

[13] A. Mwapinga, “Mathematical formulation and computation of the dynamics of blood flow, heat and mass transfer during mri scanning,” Scientific Reports, vol. 14, no. 1, p. 6364, 2024.

[14] A. Mwapinga, E. Mureithi, J. Makungu, and V. G. Masanja, “Non-newtonian heat and mass transfer on mhd blood flow through a stenosed artery in the presence of body exercise and chemical reaction,” 2020.

[15] A. Mwapinga, E. Mureithi, J. Makungu, and V. G. Masanja, “Mhd arterial blood flow and mass transfer under the presence of stenosis, body acceleration and chemical reaction: a case of magnetic therapy,” 2020.

[16] B. Thiesen and A. Jordan, “Clinical applications of magnetic nanoparticles for hyperther- mia,” International journal of hyperthermia, vol. 24, no. 6, pp. 467–474, 2008.

[17] A. Mwapinga, Computational modeling of arterial blood flow in the presence of body exercise. PhD thesis, University of Dar es Salaam, 2012.

[18] O. D. Makinde and A. S. Eegunjobi, “Effects of convective heating on entropy generation rate in a channel with permeable walls,” *Entropy*, vol. 15, no. 1, pp. 220–233, 2013.